Journal of proteome research

pubs.acs.org/jpr

Article

PPARα and PPARγ Signaling Is Enhanced in the Brain of the Naked Mole-Rat, a Mammal that Shows Intrinsic Neuroprotection from Oxygen Deprivation

Melissa R. Pergande, Vince G. Amoroso, Thu T. A. Nguyen, Wenping Li, Emily Vice, Thomas J. Park, and Stephanie M. Cologna*

Cite This: https://doi.org/10.1021/acs.jproteome.1c00131

Read Online

ACCESS | Metrics & More | Article Recommendations | Supporting Information

ABSTRACT: Naked mole-rats (NMRs) are a long-lived animal that do not develop age-related diseases including neurodegeneration and cancer. Additionally, NMRs have a profound ability to consume reactive oxygen species (ROS) and survive long periods of oxygen deprivation. Here, we evaluated the unique proteome across selected brain regions of NMRs at different ages. Compared to mice, we observed numerous differentially expressed proteins related to altered mitochondrial function in all brain regions, suggesting that the mitochondria in NMRs may have adapted to compensate for energy demands associated with living in a harsh, underground environment. Keeping in mind that ROS can induce polyunsaturated fatty acid peroxidation under periods of neuronal stress, we investigated docosahexaenoic acid (DHA) and arachidonic acid (AA) peroxidation under oxygen-deprived conditions and observed that NMRs undergo DHA and AA peroxidation to a far less extent compared to mice. Further, our proteomic analysis also suggested enhanced peroxisome proliferator-activated receptor (PPAR)-retinoid X receptor (RXR) activation in NMRs via the PPARα-RXR and PPARγ-RXR complexes. Correspondingly, we present several lines of evidence supporting PPAR activation, including increased eicosapetenoic and omega-3 docosapentaenoic acid, as well as an upregulation of fatty acid-binding protein 3 and 4, known transporters of omega-3 fatty acids and PPAR activators. These results suggest enhanced PPARα and PPARγ signaling as a potential, innate neuroprotective mechanism in NMRs.

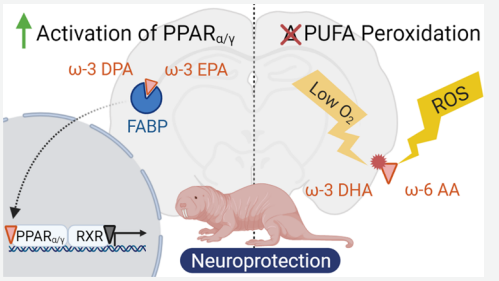

KEYWORDS: *naked mole-rat, mass spectrometry, ω-3 docosapentaenoic acid, eicosapentaenoic acid, lipid peroxidation, FAHFA, PPARα, PPARγ*

INTRODUCTION

Heterocephalus glaber, or the naked mole-rat (NMR), is a subterranean species indigenous to portions of eastern Africa that live in eusocial colonies of up to several hundred individuals in underground burrows where they spend their entire lives.[1] Living in a large social colony is very unusual among subterranean mammals and, thus, has presumably allowed for the development of multiple adaptive features including their resistance to hypoxia. In general, numerous individuals sharing the same limited air supply results in depletion of oxygen and accumulation of carbon dioxide. Consistent with living in this challenging environment, the NMR demonstrates a constellation of unusual physiological features.[2] In previous studies, we have demonstrated that NMRs can live for 18 minutes without oxygen,[3] and in vitro hippocampal slices maintain functionality for over 40 minutes without oxygen.[4] These in vivo and in vitro survival times far surpass those of similar-sized rats and mice. Additionally, it was observed that NMRs are unique in their ability to switch from an aerobic metabolism of glucose to an anaerobic metabolism of fructose to supply energy to the heart and brain during oxygen deprivation.[3] Interestingly, the NMR is also resistant to the deleterious effects of breathing high concentrations of carbon dioxide, where no pulmonary edema is observed in response to the acidic respiration.[3] Moreover, NMRs are the only poikilothermic mammal, lacking the ability to generate appreciable body heat, which drastically reduces the demand for oxygen-derived energy. Further, NMRs assume the ambient temperature of their surroundings, which in their burrows can vary ±2 °C, depending on the time of day, location in the burrow system, or proximity to other NMRs.[5] Notably, their preferred temperature is roughly 30 °C.[6]

Among the most striking features of the NMR is their ability to survive oxidative insult and resistance to age-related neurodegenerative diseases. At 32 years, the NMR holds the

Received: February 14, 2021

record for longest-lived rodent and is an outlier when the relationship between body size and longevity is considered.[7] Compared to mice (similar body mass), the NMR lives roughly an order of magnitude longer (e.g., 3 vs 30 years). While the mechanisms underlying such longevity are currently unknown, genomic sequencing of the NMR has revealed upregulation of several pathways related to mitochondrial function and oxidative species reduction,[8,9] as well as fatty acid metabolism.[10] It has been shown that even from a young age, NMRs exhibit high levels of reduced oxidative stress where several markers associated with lipids (i.e., isoprostanes and malondialdehyde (MDA)), proteins (protein carbonyls and cysteine oxidation), and DNA (8-oxo-2'deoxyguanosine (8-OHdG)) have been reported to be altered in several tissues including the brain,[11] despite their high load of reactive oxygen species (ROS). Munro and colleagues observed that mitochondria in NMRs were able to consume ROS at a much higher rate than mice.[12] Saldmann and colleagues also noted the lower basal antioxidant levels in NMRs relative to mice including evidence of CuZnSOD, catalase, thioredoxin, glutathione (GSH), and glutathione reductase levels.[13] In fact, Lewis and colleagues observed that cellular glutathione peroxidase levels were 70-fold lower in NMRs compared to mice.[11] Further, these authors also observed lower levels of GSH, similar glutathione disulfide (GSSG) levels and an overall lower GSH/GSSG ratio in NMRs.

To date, there are only a few proteomic studies reported in the literature that are aimed at understanding the unique attributes of NMRs. Triplett and colleagues used two-dimensional gel electrophoresis and mass spectrometry to evaluate age-related changes in the proteostasis network of the brain and showed that autophagy is upregulated in NMRs throughout most of their lifespan, perhaps contributing to their extraordinary health and tolerance to aging.[14] Triplett and colleagues also explored the metabolic pathways related to longevity and identified phosphorylation sites of specific proteins underlying enhanced neurite outgrowth and neurotransmission in NMRs.[15] Heinze and colleagues also evaluated the liver proteome of the NMR and found a unique expression pattern of mitochondrial proteins that results in distinct metabolic features of their mitochondria.[16] Frankel and colleagues observed that proteins involved in ceramide, sphingomyelin, and sphingosine-1-phosphate metabolism were decreased in NMRs relative to mice.[17] More recently, Guan and colleagues identified plasma proteomes of mice and NMRs and evaluated different times points to investigate circadian changes as well as effects of UV irradiation.[18] Although these studies are very insightful, there remains a knowledge gap regarding the proteome of the NMR brain. Therefore, we sought to evaluate the altered proteome of NMRs relative to mice to elucidate proteins that may be involved in the unique neurobiology and disease resistance of the NMR, such as those described above.

With a focus on the brain, in the present work, we highlight multiple proteomic alterations supporting previous observations of the altered mitochondrial function in NMRs. Additionally, we observed that NMRs undergo docosahexaenoic acid (DHA) and AA peroxidation to a far less extent compared to mice, also supporting our observation of altered mitochondrial function in NMRs. Finally, we present several lines of evidence suggesting enhanced PPARα and PPARγ signaling as an innate neuroprotective mechanism in NMRs.

MATERIALS AND METHODS

Reagents and Chemicals

Lipid standards of 4-hydroxyhexenal (4-HHE), 4-hydroxynonenal (4-HNE), 4-hydroxyhexenal-d_3 (4-HHE-d_3), and 4-hydroxynonenal-d_3 (4-HNE-d_3) were purchased from Cayman Chemical Co. (Ann Arbor, MI). Stearic (SA), palmitic (PA), oleic (OA), ω-6 linoleic acid (LA), ω-6 γ linolenic (DGLA), ω-6 arachidonic (AA), ω-6 docosatetraenoic (DTA), ω-6 docosapentaenoic (ω-6 DPA), ω-3 eicosapentaenoic (EPA), ω-3 docosapentaenoic (ω-3 DPA), and ω-3 docosahexaenoic (DHA) acid standards were obtained from Nu-check (Elysian, MN). All other reagents were obtained from Sigma-Aldrich (St. Louis, MO) and used as received unless otherwise noted.

Animal Studies and Tissue Collection

All animal experiments were performed according to institutional animal care and use committee-approved protocols. Both males and females and mature and young animals of C57BL/6 mice and NMRs were used. Mice were conventionally housed with nesting material in temperature-controlled rooms at 21 °C, with a 12 h light/dark cycle and access to food and water ad libitum. NMRs were bred in-house and maintained in an interconnected network of cages in a temperature-controlled room at 28 °C and had access to food ad libitum. For differential proteomic studies, animals from each species were selected, which represent a range of ages, including both mature and young ages of each. Here, mice were euthanized at 2 weeks (young mice, $N = 4$) and 2 months (mature mice, $N = 4$) of age. Similarly, NMRs were euthanized at 2 months (young NMR, $N = 4$) or 3 years (mature NMR, $N = 4$) of age. Given that the areas of the brain have been observed to be affected differentially in various neurological disorders, each brain tissue was dissected and divided into three main subtypes (cerebellum, cortex, and hippocampus) and flash frozen, as previously described.[19−21] For oxygen-deprivation studies on select targets, a separate set of animals were maintained either at normoxic (21% O_2) or in a hypoxic atmosphere (10% O_2 for mice, 5% O_2 for NMR) for 24 h prior to tissue collection. In this portion of the study, $N = 4$ (mice) and $N = 3$ (mole-rat) were used for each condition.

Tissue Lysis and LC-MS Sample Preparation

Protein extracts for each tissue (cerebellum, cortex, and hippocampus) from each animal were prepared and analyzed via liquid chromatography-mass spectrometry (LC-MS) analysis (Figure S1). Protein extracts were obtained via tissue lysis in RIPA buffer (50 mM Tris pH 8, 150 mM NaCl, 1% Triton X-100, 0.5% sodium deoxycholate, 0.1% sodium dodecylsulfate). Protein concentration was determined via a bicinchoninic acid (BCA) assay (Pierce-Thermo, San Jose, CA). Next, peptide digests from 100 μg of protein were prepared for each of the tissue lysates using the filter-aided sample preparation (FASP) method after spiking in a recombinant green fluorescent protein (GFP) internal standard into each sample at a concentration of 100 fmol per 1 μg protein extract as previously described.[19] Finally, samples were desalted via C18 reversed-phase chromatography and dried in vacuo. All samples were resuspended in 100 μL 0.1% (v/v) formic acid prior to LC-MS analysis.

LC-MS Analysis

One microliter of each sample was injected for label-free, quantitative LC-MS analysis. Mass detection was carried out with a Q-Exactive mass spectrometer (Thermo Fisher

https://doi.org/10.1021/acs.jproteome.1c00131
J. Proteome Res. XXXX, XXX, XXX−XXX

Scientific, Bremen, Germany) equipped with an Agilent 1260 nano/capillary high-pressure liquid chromatography system. Chromatographic separation of peptides was accomplished using a Zorbax 300SB-C18 column (3.5 μm i.d. × 150 mm, particle size 5 μm, pore size 100 Å, Agilent Technologies, Wilminton, DE). Peptides were loaded onto a Zorbax 300SB-C18 trap cartridge (Thermo Pierce Biotechnology, Rockford, IL) at a flow rate of 2 μL/min for 10 min. After washing with 0.1% formic, the peptides were eluted using a 5−40% B gradient for 180 min at a flow rate of 250 nL/min for a total LC-MS analysis time of 240 min per sample, where mobile phase A was 0.1% formic acid and mobile phase B was 0.1% formic acid in acetonitrile. The mass spectrometer was operated in data-dependent mode with automatic switching between MS and MS/MS with HCD fragmentation for the top 10 precursors. Source ionization parameters were as follows: spray voltage, 1.5 kV; capillary temperature, 280 °C, and s-lens level, 50.0. Full-scan MS mode (m/z 300−1700) was operated at a resolution of 70 000 with automatic gain control (AGC), a target of 1×10^6 ions, and a maximum ion transfer (IT) of 250 ms. Ions selected for MS/MS were subjected to the following parameters: resolution, 17, 500; AGC, 1×10^5 ions; maximum IT, 100 ms; m/z 1.5 isolation window; normalized collision energy 27.0 V; and dynamic exclusion, 30 s. All raw mass spectrometry data is publicly available at https://massive.ucsd.edu/ProteoSAFe/static/massive.jsp using project ID MSV000086617.

Data Analysis

The NMR and mice genomes share 83% homology;[22] therefore, raw data for the LC-MS analysis of each sample was searched against both the UniProt *Mus musculus* (25 230 sequences) and *Heterocephalus glaber* (27 180 sequences) databases in addition to an in-house GFP database were using the Proteome Discoverer software (v2.3, Thermo Fisher, Carlsbad, CA). Here, trypsin was set as the protease with two missed cleavages and searches were performed with precursor and fragment mass error tolerances set to 10 ppm and 0.02 Da, respectively, where only peptides precursors of +2, +3, and +4 were considered. Peptide variable modifications allowed during the search were oxidation (M) and deamination (NQ), whereas carbamidomethyl (C) was set as fixed modifications. In the Proteome Discoverer software, samples were grouped according to the following study factors: tissue type (cerebellum, cortex, or hippocampus) and species (NMR (N = 8) or mice (N = 8)) (Figure S2). Identified proteins for each species were evaluated to determine whether reasonable proteome coverage could be obtained for both NMRs and Mice using either the *Mus Musculus* or *Heterocephalus glaber* database. Next, a label-free relative quantitation analysis was performed using a peptide precursor-based (MS1) quantification workflow. Briefly, the Minora Feature Detector node was used where LC-MS peaks in the raw data were mapped to identify PSMs by fitting the observed isotope pattern to the theoretical. Next, the Precursor Ion Quantifier node was used for relative quantification where the summed abundance of peptide groups was selected. In this workflow, both razor and unique peptides were used with no imputation of missing values. Protein abundancies were normalized across all samples and all tissues using the intensity of GFP. Differentially expressed proteins for NMRs relative to mice for each tissue type were determined by applying an unpaired t-test and Benjamini−Hochberg correction for the false-discovery rate ($p \leq 0.05$). To determine whether significant proteomic alterations were attributed to tissue type, a principle component analysis was performed. Biological relevance was determined for altered proteins using the Ingenuity Pathway Analysis software (IPA, Ingenuity Systems, Redwood City, CA) where a right-tailed Fisher's exact test was used to calculate a p-value to determine the probability for both pathways and disease and biological function analysis from the IPA Knowledge Base Library to those most significantly enriched.

Western Blot Analysis

Protein lysates were subject to electrophoresis and Western blotting for select protein targets. The samples were heated in Laemmli buffer containing DTT at 90 °C for 10 min before loading onto a 12% NuPage Bis-Tris gel (Novex Life Technologies, Carlsbad, CA). Proteins were separated by SDS-PAGE (120 V for ∼120 min) and transferred to nitrocellulose membrane via a Wet Transfer blotting apparatus (Novex Life Technologies, Carlsbad, CA) at 10 V for 60 min. Membranes were blocked in a solution of 5% (wt/v) dry milk and 0.1% (v/v) Tween-20 (PBS-T) overnight before the addition of primary antibody followed by the addition of the secondary antibody in 5% (wt/v) milk PBS-T for 1 h. Excess secondary antibody was removed by washing three times with PBS-T before protein bands were visualized by incubation with Pico West Blotting Substrate (Thermo Pierce Biotechnology, Rockford, IL) and imaging on an Azure c300 imaging system (Dublin, CA). Western blot signals were compared via densitometry analysis using ImageJ (http://rsb.info.nih.gov/ij/index.html). GraphPad Prism (v9.0.0) was used to determine statistical significance. Details regarding Western blot reagents are provided in Table S1. All raw Western blot images are publicly available at the following link: https://massive.ucsd.edu/ProteoSAFe/static/massive.jsp using project ID MSV000086617).

Lipid Peroxidation Assays

Lipid peroxidation was investigated in both species under normoxic and hypoxic conditions. First, levels of malondialdehyde (MDA) were measured using a colorimetric assay (Abcam ab233471, Cambridge, MA), where concentrations were determined via the generation of a standard curve (Figure S3A). Next, to determine whether lipid peroxidation was specific to AA and/or DHA, a LC-MS assay was developed as previously described.[23] Here, a standard curve was generated for the 4-HHE (Figure S3B) and 4-HNE (Figure S3C) derivatives. Briefly, 1 μg of 4-HHE and 4-HNE were derivatized by adding 200 μL of derivatization mixture (200 mM 1,3-cyclohexanedione (CHD), 1.3 M ammonium acetate, and 3.5 M acetic acid) and incubated at 70 °C for 1 h (Figure S4A). Derivatized 4-HHE and 4-HNE were then desalted using a C18 SPE cartridge and the eluate dried in a vacuum centrifuge and resuspended in 200 μL of ethanol. Next, brain tissue samples were homogenized in 1× phosphate-buffered saline (PBS) solution and protein concentration was measured via a BCA assay. Aliquots (100 μg protein equivalent) of each tissue lysate were spiked with 1 ng of both 4-HHE-d_3 and 4-HHE-d_3 and samples were derivatized in the same manner as described above. After drying, samples were resuspended in 10% acetonitrile containing 0.1% formic acid and analyzed on an Agilent 6550 iFunnel Q-TOF LC/MS system. The mass spectrometer was operated in the 2 GHz extended dynamic range mode employing data-dependent acquisition for the top

https://doi.org/10.1021/acs.jproteome.1c00131
J. Proteome Res. XXXX, XXX, XXX−XXX

5 precursors in positive ion mode and internal reference mass calibration ions m/z 121.0509 and 922.0098. Mobile phase A was 0.1% formic acid and B was acetonitrile with 0.1% formic acid. The derivatized standards and samples were loaded onto a 2.1 × 100 mm Agilent Zorbax RRHD C18, 1.8 μm column (Agilent Technologies Inc., Santa Clara, CA) and separation performed on an Agilent 1290 UPLC system using the following gradient: 10% B at 0 min, 50% B at 5 min, 90% B at 5.1 min, and hold at 90% B until 8 min followed by a 4 min post analysis equilibration at 10% B. Data-dependent acquisition was performed on the top 5 precursors at a scan speed of MS (m/z 100−1000) at 6 spectra per second and MS/MS at 3 spectra per second using a m/z 1.3 isolation window and 25 V collision energy. Source parameters were as follows: gas temperature, 150 °C; drying gas flow, 11 L/min; nebulizer, 50 psi; sheath gas temperature, 350 °C; sheath gas flow, 12 L/min: capillary voltage, 3500 V; nozzle voltage, 500 V and fragmentor, 125 V. Five microliters of each of the samples were injected for analysis. Peak areas were manually extracted for derivatized analytes 4-HHE (Figure S4B), 4-HNE (Figure S4C), 4-HHE-d_3 (Figure S4D), and 4-HNE-d_3 (Figure S4E) in the Mass Hunter Qualitative Analysis software (Agilent Technologies Inc., Santa Clara, CA) and fragmentation matched. Peak areas for both 4-HHE and 4-HNE were normalized to their respective deuterated internal standards. Data was plotted and statistical analysis was performed using GraphPad Prism (v9.0.0). All raw mass spectrometry data was deposited and is publicly available at https://massive.ucsd.edu/ProteoSAFe/static/massive.jsp using project ID MSV000086617.

Analysis of Fatty Acids

Stock solutions of fatty acid standards (PA, SA, OA, LA, DGLA, AA, DTA, ω-DPA, EPA, ω-3 DPA, and DHA) were made at 1 pg/μL in 20% acetonitrile. Aliquots (100 μg protein equivalent) of each of the brain tissues were homogenized in 500 μL of methanol containing 25 mM of HCL. Two hundred picograms of palmitic acid-16, 16, 16-d_3 (PA-d_3) internal standard was added to each sample. Next, 1 mL of iso-octane was added, samples vortexed, and spun at 3000g to separate the layers. The iso-octane layer (top) was removed and transferred to a new tube. The iso-octane extraction was repeated once, iso-octane layers combined, and fatty acid extracts dried in a vacuum centrifuge at 35 °C. Samples were resuspended in 200 μL of 20% acetonitrile and 5 μL of the standard mix, and each of the samples was analyzed in a similar manner to the lipid peroxidation products in negative ion mode. Here, internal reference mass calibration ions m/z 112.9855 and 980.0163 were used and mobile phase A was 0.1% acetic acid with 5 mM ammonium acetate and B was 7:3 acetonitrile/2-propanol with 0.1% acetic acid and 5 mM ammonium acetate. Analytes were separated using the following gradient: 70% B at 0 min, 86% B at 15 min, 90% B at 15.1 min, and hold at 90% B until 17 min followed by a 3 min post analysis equilibration at 70% B at a flow rate of 0.35 mL/min. Data-dependent acquisition was performed on the top 5 precursors at a scan speed of MS (m/z 100−1000) at 6 spectra per second and MS/MS at 3 spectra per second using a m/z 1.3 isolation window and 30 V collision energy. Additional fatty acid species were identified using the Lipid Annotator software (Agilent Technologies Inc., Santa Clara, CA) using a Q-score > 60, and mass deviation ≤5 ppm. Each of the integrated peaks was manually reviewed for retention time and fragmentation matching. Peak areas were manually extracted for all fatty acid species in the Mass Hunter Qualitative Analysis software (Agilent Technologies Inc., Santa Clara, CA). All peak areas were normalized to the PA-d_3 internal standard. Data was plotted and statistical analysis was performed using GraphPad Prism (v9.0.0). All raw mass spectrometry data was deposited and is publicly available at https://massive.ucsd.edu/ProteoSAFe/static/massive.jsp using project ID MSV00086617.

RESULTS AND DISCUSSION

Brain Proteomic Analysis via LC-MS

NMRs are known to possess a highly unusual set of neurological traits including intrinsic brain tolerance to oxygen deprivation,[4] failure to develop amyloid plaques in aged animals,[24] and resistance to neurogenic pulmonary edema from breathing high concentrations of CO_2 while thriving in a harsh underground environment.[3] In the present study, we analyzed the proteome of the NMR by LC-MS with a focus on the cerebellum, cortex, and hippocampus regions. To gain insight into whether specific proteins found in our analysis could be related to some of the unique neurological attributes of the NMR species, we aimed to compare the relative expression of our measured proteome to a cohort of mice. In the first part of our analysis, we compared the number of protein groups identified across the different tissues using the *Mus musculus* and *Heterocephalus glaber* databases. Using the *Mus musculus* database, 2264, 2025, 2241, 1871, 2315, and 1868 protein groups were identified in the mouse cerebellum, NMR cerebellum, mouse cortex, NMR cortex, mouse hippocampus, and NMR hippocampus, respectively (Table S2, Figure S5A). Using the *Heterocephalus glaber* database, 1916, 2290, 1903, 2192, 1956, and 2198 protein groups were identified in the mouse cerebellum, NMR cerebellum, mouse cortex, NMR cortex, mouse hippocampus, and NMR hippocampus, respectively (Table S2, Figure S5B). In this study, we observed an overlap > 80% in proteins identified between species in each tissue type using either database.

A label-free relative quantification analysis was carried out to identify altered proteins in the cerebellum, cortex, and hippocampus of NMRs relative to mice (Table S2). First, evaluation of the differential proteome was performed of raw data analyzed via the *Mus musculus* database. This analysis revealed 563, 542, and 561 proteins significantly altered in the cerebellum, cortex and hippocampus, respectively. Second, evaluation of the differential proteome was performed of raw data analyzed via the *Heterocephalus glaber* database. This analysis revealed 552, 538, and 543 proteins significantly altered in the cerebellum, cortex, and hippocampus, respectively. Next, a principle component analysis was performed for altered proteins observed upon analysis of raw data searched against both the *Mus musculus* (Figure S6A) and *Heterocephalus glaber* (Figure S6B) databases. In both cases, it was observed that one main component was not strongly driving the significant alterations of proteins. On the other hand, altered proteins from the same species clustered together regardless of tissue type, indicating that the main difference driving these alterations is most likely attributed to the divergence of species. Additionally, the altered proteome search against the *Mus musculus* database was plotted where volcano plots revealed a symmetrical distribution of altered proteins (both up and downregulated) in each tissue type

https://doi.org/10.1021/acs.jproteome.1c00131
J. Proteome Res. XXXX, XXX, XXX−XXX

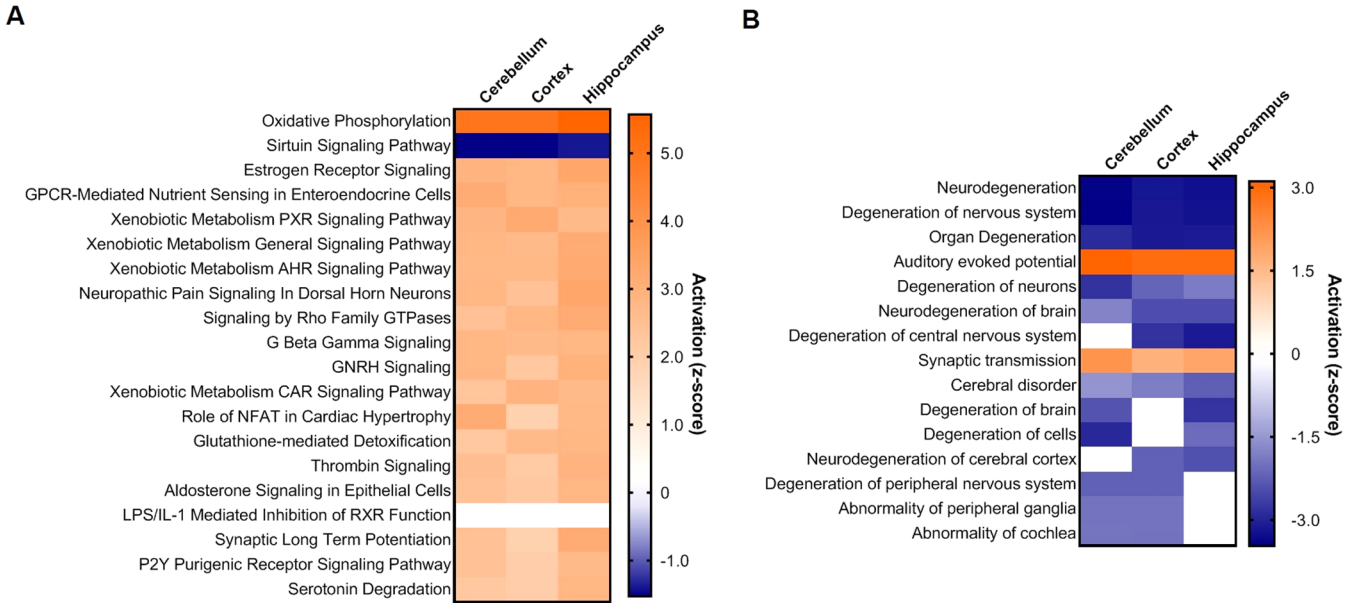

Figure 1. Ingenuity Pathway Analysis of the altered proteome observed between mice and naked mole-rats. (A) Top-ranked (top 20) conical pathways and (B) disease and functional processes of the cerebellum, cortex, and hippocampus tissues for significantly altered proteins measured in naked mole-rats ($N = 8$) relative to mice ($N = 8$). Activation is depicted as a z-score, where blue is downregulated, orange is upregulated, and white is no regulation pattern predicted.

(Figure S7). To elucidate the biological relevance of the altered proteomes of each brain tissue from NMRs, we performed pathway (Table S3) and biological function (Table S4) analysis for proteins found to be significantly altered relative to mice using the results obtained from the analysis using the *Mus Musculus* database.

Altered Mitochondrial Function

It is not surprising that many of the top-ranked pathways across all brain regions are associated with the mitochondria, as NMRs are well known to have altered mitochondrial function relative to other species such as mice.[12] Our proteomic analysis revealed altered pathways relating to oxidative phosphorylation, mitochondrial dysfunction, sirtuin signaling, and glutathione-mediated detoxification (Figure S8, Figure 1A). Interestingly, Munro and colleagues observed that the mitochondria's ability to consume ROS was markedly greater in NMRs compared to mice.[12] We observed alterations in numerous mitochondrial proteins including ATP synthase, cytochrome c oxidase, NADH dehydrogenase, and ubiquinol-cytochrome *c* oxidoreductase proteins, all associated with increased oxidative phosphorylation and in agreement with previous reports.[25] Sirtuin signaling plays an important role in aging, metabolism, cancer, inflammation, DNA repair, and cellular responses to stress.[26] Here, we observed numerous proteins throughout this pathway that were altered in NMRs including superoxide dismutase [Cu-Zn] (SOD1) and NAD-dependent protein deacetylase sirtuin-2 (SIRT2). Consistent with ROS tolerance, SOD1 was decreased in NMRs (cerebellum ratio: 0.1, $p = 2 \times 10^{-8}$; cortex ratio: 0.03, $p = 1 \times 10^{-17}$; hippocampus ratio: 0.05, $p = 1 \times 10^{-17}$) presumably due to the NMR's ability to consume ROS and, thus, preventing a buildup and subsequent toxic cellular effects. Given the decreased load of ROS, it is reasonable to infer that detoxification mechanisms such as those that involve SOD1 may be less active in NMRs. Moreover, SIRT2 was also decreased in the hippocampus (ratio 0.36, $p = 0.006$) as well as the cerebellum and cortex (although not observed to be significant). Interestingly, SIRT2 has been reported to modulate a multitude of diverse biological processes such as aging, cell cycle control and differentiation, apoptosis, and autophagy.[27] Further, numerous reports in the literature suggest that SIRT2 inhibition rescues neurodegenerative disease symptoms and may serve as a potential therapeutic target for neurodegenerative disease.[27−29] One study reported that increased expression of SIRT2 was observed in NMRs under hypoxic conditions, perhaps contributing to neuronal survival.[30] Finally, we also observed an alteration in numerous transferase enzymes including glutathione S-transferase Mu 1, glutathione S-transferase Mu 3, glutathione S-transferase Mu 5, and glutathione S-transferase omega-1. Glutathione degradation enzymes are necessary to maintain low levels of ROS and are consistent with previous observations indicating a pro-oxidative environment in NMRs.[31] In these cases, many of these enzymes were decreased; however, this differs by tissue type and varying levels of significance (see Table S2). Notably, ROS cause oxidative stress, damaging mitochondria that triggers neurodegenerative diseases and accelerates aging.[32] Taken together, our results support the idea that the mitochondria of NMRs are engineered to maintain low levels of ROS, perhaps contributing to the neotenic characteristic of this species.[4,33]

Decreased Amounts of Proteins Associated with Neurodegeneration

NMRs are a long-lived species much like humans but have a profound ability to withstand numerous neurodegenerative diseases.[24,34] As such, we hypothesized that the differential proteome would reveal insights into processes related to neurodegeneration. As expected, our disease and biological function analysis revealed the downregulation of numerous disease processes relating to neurodegeneration and demyelination (Figure 1B). These data suggest that NMRs may have multiple mechanisms by which they are able to prevent the loss

https://doi.org/10.1021/acs.jproteome.1c00131
J. Proteome Res. XXXX, XXX, XXX−XXX

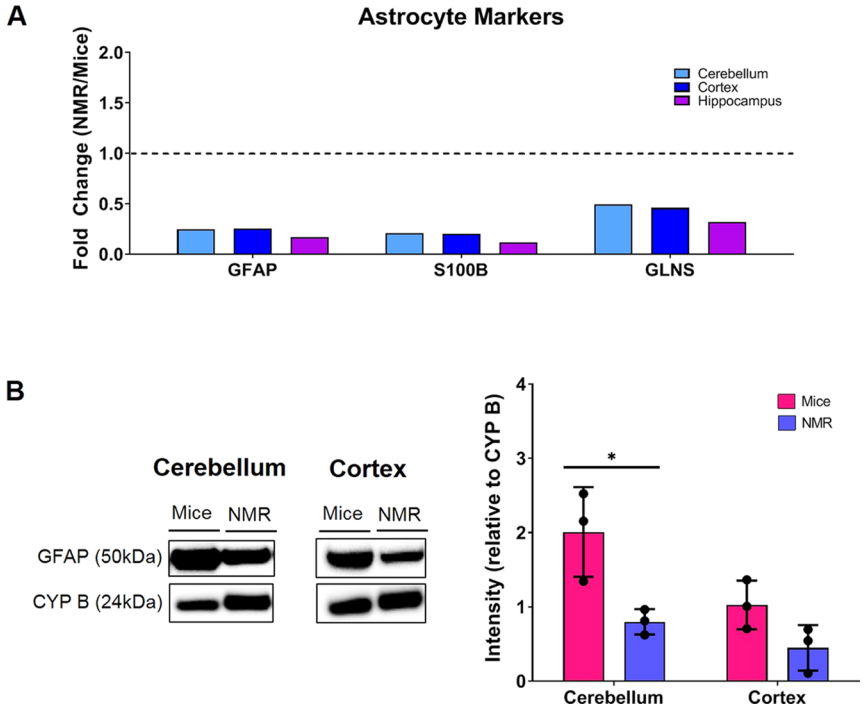

Figure 2. Relative abundance of astrocyte markers in mice and naked mole-rats. (A) Bar graphs showing mass spectrometry analysis of selected astrocyte protein markers across tissue types (cerebellum, cortex, and hippocampus) in naked mole-rats and mice for glial fibrillary acidic protein (GFAP), protein S100-B (S100B), and glutamine synthetase (GLNS). (B) Tissue lysates were subject to electrophoresis and Western blotting for both mice and NMRs to evaluate the expression of GFAP in the cerebellum and cortex via Western blot. Intensity is relative to cyclophilin B (CYP B). Representative plots of mean intensity are shown, where $N = 4$ mice and $N = 3$ NMRs for each condition; blots for individual animal can be seen in Figure S9. Significance for (B) is noted as $p \leq 0.05$ (*).

of neurons, contributing to the diversity and vast number of proteins reflecting the downregulation of neuronal death (Table S4). When reviewing proteins found to be decreased among the above-mentioned disease processes, it was observed that multiple astrocyte markers were decreased across all tissues in the NMR including glial fibrillary acidic protein (GFAP), protein S100-B (S100B), and glutamine synthetase (GLNS) (Figure 2A). During periods of neuronal hyperactivity, mitochondria generate numerous ROS. In response, fatty acids, such as the polyunsaturated fatty acid (PUFAs), become peroxidated and are transferred via lipid particles (e.g., APOE) to astrocytes, where peroxidated fatty acids are detoxified as a means of maintaining neuronal integrity.[35] Notably, we also observed decreased levels of APOE across all tissues in NMRs (Table S3). With this, we performed an orthogonal analysis of GFAP, where Western blot analysis also revealed lower expression in NMRs relative to mice in the cerebellum and cortex (Figure S9, Figure 2B). We posit that one reason for the possible decrease in astrocytes may be attributed to the decreased need for peroxidated fatty acid detoxification. Further histological studies across the different regions of the brain in NMRs would be needed to evaluate the ratio of astrocytes per a given density of neurons to better understand the observations of decreased astrocytic markers. Taken together, the results of the present study suggest that under conditions known to induce high levels of ROS, such as oxygen deprivation, NMR brain cells have established molecular mechanisms allowing for the tolerance of such environments better than mice.

Fatty Acid Peroxidation under Hypoxic Conditions

PUFAs are among the molecules most susceptible to peroxidation by ROS.[36] Building on our hypothesis of decreased astrocytes in NMRs, we explored the levels of peroxidated PUFAs under conditions known to induce ROS. Here, we obtained brain tissues from animals held at normoxic (21% oxygen) and hypoxic conditions for both mice (10% oxygen) and NMR (5% oxygen) species. A lipid peroxidation assay to measure the reactive aldehyde product malondialdehyde (MDA, known lipid peroxidation marker) was carried out, where the amount of MDA was determined across different brain regions (Figure 3A). An increase in MDA was observed for mice under hypoxic conditions in both the cerebellum and cortex, while no significant change was observed in the hippocampus. A higher level of MDA was also observed in NMRs relative to mice in the cerebellum under normoxic conditions. To determine whether this peroxidation was specific to the DHA or AA, the peroxidation products 4-hydroxyhexenal (4-HHE, specific for DHA) and 4-hydroxynonenal (4-HNE, specific for AA) were measured in the cerebellum (Figure 3B), cortex (Figure 3C), and hippocampus (Figure 3D). In both the cerebellum and cortex, we observed an increase in both 4-HHE and 4-HNE in mice under hypoxic conditions. In the cerebellum, we also observed an increase in both peroxidation products in NMRs relative to mice under normoxic conditions, specific to the cerebellum. On the other hand, we observe an increase in 4-HNE in NMRs compared to mice under hypoxic conditions in both the cerebellum and cortex and an increase of 4-HHE in the cortex only.

https://doi.org/10.1021/acs.jproteome.1c00131
J. Proteome Res. XXXX, XXX, XXX−XXX

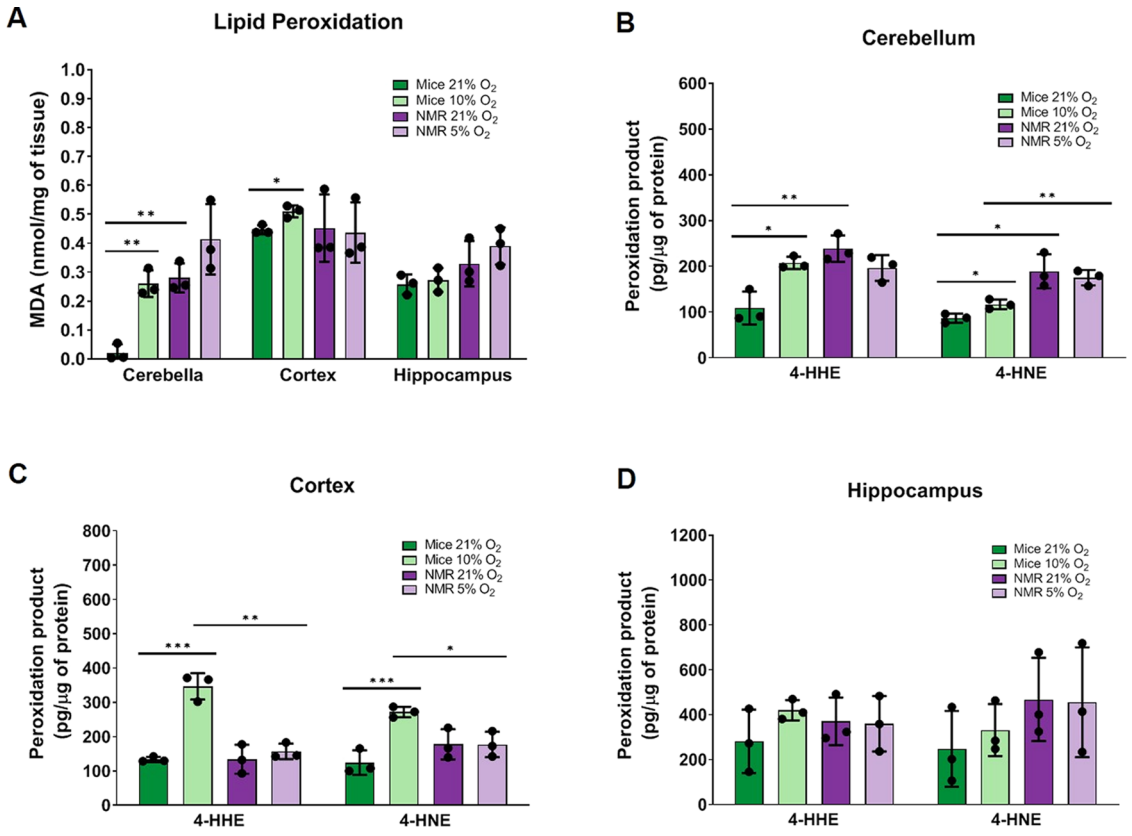

Figure 3. Lipid peroxidation analytes measured in the brain of mice and naked mole-rats. Brain tissues were obtained from animals held at normoxic (21% O_2) and hypoxic conditions for both mice (10% O_2) and naked mole-rats (NMR) (5% O_2). (A) A lipid peroxidation assay to measure the reactive aldehyde product malondialdehyde (MDA) was carried out. An increase in MDA was observed for mice under hypoxic conditions in both the cerebellum and cortex, while no change is observed in the hippocampus. Higher levels of MDA were also observed in NMRs in the cerebellum under normoxic oxygen conditions. Peroxidation products 4-hydroxyhexenal (4-HHE, specific for docosahexaenoic acid (DHA)) and 4-hydroxynonenal (4-HNE, specific for arachidonic acid (AA)) were measured in the (B) cerebellum, (C) cortex, and (D) hippocampus. The amount of MDA was normalized to the weight of the tissue and levels of 4-HHE and 4-HNE were normalized to protein content. Significance was determined using an unpaired t-test between each condition and species. Significance for (A)−(D) is noted as $p \leq 0.05$ (*), $p \leq 0.01$ (**), and $p \leq 0.001$ (***).

ROS are rapidly neutralized to maintain a proper balance between the rate of production and the rates of detoxification in healthy tissues, whereas an excess of ROS, resulting from either overproduction or insufficient activity of antioxidation, leads to oxidative stress and many disease processes such as cancer, aging, and neurodegenerative diseases.[37] Interestingly, the PUFAs are very sensitive to oxidation, an action of ROS, as they are common constituents of phospholipids which are abundant in numerous cell membranes. This can pose a problem for cells, specifically neurons, as the accumulation of peroxidated lipids can lead to toxic cellular products, if accumulated in high concentrations. The observations from our experiments suggest that NMRs have the innate ability to detoxify ROS in brain tissues. Therefore little change in peroxidation of PUFAs compared to mice is observed, even under hypoxic conditions, perhaps as a result of an adaption by neuronal mitochondria to consume ROS. Moreover, these data are consistent with our observation of decreased astrocyte markers in NMRs, as there would be a decreased need for peroxidated fatty acid detoxification. Taken together, we consider that neuronal mitochondria in NMRs may be uniquely engineered to compensate for increased ROS consumption, possibly structurally or via extensive depolarization.[38] Further, we believe that this attribute may have evolved in NMRs to survive their oxygen-deprived burrows; however, further experiments would be needed to test this hypothesis.

Activation of PPAR Receptors

Common across all tissues was the alteration of lipopolysaccharide (LPS)/interleukin (IL)-1 mediated inhibition of retinoid X receptor (RXR) function (Figure 1A). RXR is a type-II, ligand-dependent nuclear receptor that forms a complex with other ligand-dependent nuclear receptors, such as peroxisome proliferator-activated receptors (PPARs), which also activate numerous transcriptional receptors.[39] LPS and IL-1 are known to trigger the inhibition of these transcriptional cassettes.[40] Increased PPAR-RXR function can lead to altered metabolism, transport, or biosynthesis of cholesterol and xenobiotics.[41,42] Interestingly, we found that proteins related to cholesterol biosynthesis and xenobiotic metabolism (Figure 1A) were mainly upregulated, consistent with previous observations.[17] Further, several lines of evidence have established an association between neurodegenerative diseases and type-II nuclear receptors, namely, the RXR, retinoic acid receptor (RAR), liver X receptor (LXR), and PPARs.[43,44]

PPARs play crucial roles in multiple cell types including neurons and consist of multiple subtypes, PPARα, PPARβ, and PPARγ. In general, PPARs display a broad range of selectivity including long-chain fatty acids.[45,46] Notably, PPAR agonists

https://doi.org/10.1021/acs.jproteome.1c00131
J. Proteome Res. XXXX, XXX, XXX−XXX

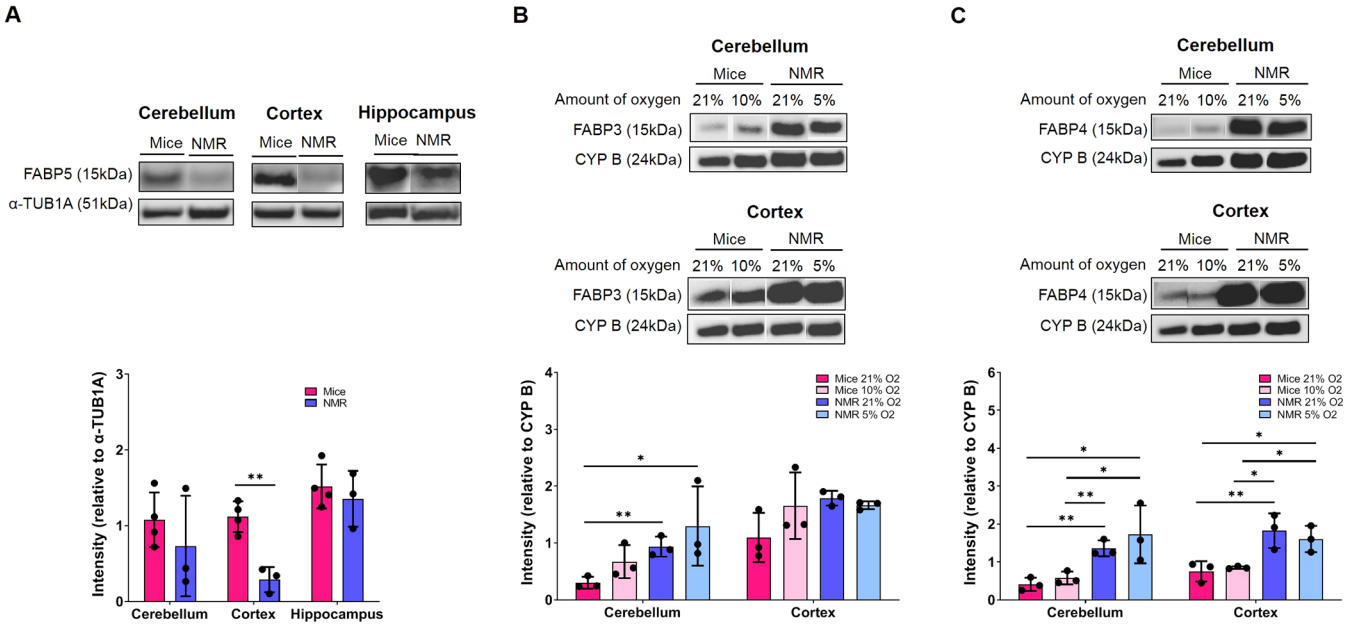

Figure 4. Western blot analysis of fatty acid-binding proteins in the brain tissue of mice and naked mole-rats. Tissue lysates were subject to electrophoresis and Western blotting for both mice and naked mole-rats (NMR) to evaluate the expression of fatty acid-binding proteins in brain tissue. (A) Evaluation of the relative expression of fatty acid-binding protein 5 (FABP5) in the cerebellum, cortex, and hippocampus. (B) Evaluation of the relative expression of fatty acid-binding protein 3 (FABP3) in the cerebellum and cortex under normoxic (21% O_2) and hypoxic conditions for both mice (10% O_2) and naked mole-rats (NMR) (5% O_2). (C) Evaluation of the relative expression of fatty acid-binding protein 4 (FABP4) in the cerebellum and cortex under normoxic (21% O_2) and hypoxic conditions for both mice (10% O_2) and naked mole-rats (NMR) (5% O_2). Fold change for each is reported as relative to α-tubulin (α-TUB1A) for FABP5 and cyclophilin B (CYP B) for FABP3 and FABP4. Significance was determined via an unpaired t-test between all possible pairs of conditions in (A)−(C). Representative plots of mean intensity are shown, where $N = 4$ mice and $N = 3$ NMRs for each condition, where blots for individual animals can be seen in Figures S12−S14. Significance for (A)−(C) is noted as $p \leq 0.05$ (*) and $p \leq 0.01$ (**).

must traverse the plasma membrane, cytoplasm, and nuclear membrane to activate their nuclear receptors. The fatty acid-binding proteins (FABPs) are small, soluble proteins that transport fatty acids into the nucleus to activate PPARs.[47] In the present study, we measured the relative abundance of numerous FABPs in our mass spectrometry analysis (Figure S10). We observed increased FABP1 in the cerebellum and hippocampus, increased FABP3 in the cortex and hippocampus, decreased FABP5 in all tissues, and increased FABP7 in the hippocampus. Interestingly, Tan and colleagues observed that FABPs enhance the transcriptional activity of PPARs with strict selectivity for the receptor, where FABP3, FABP5, and FABP4 enhanced the transcriptional activity of PPARα, PPARβ, and PPARγ, respectively.[48] Together with our observations, this suggests that PPARα and PPARγ activation is increased in specific NMR brain regions, while PPARβ activation is repressed in all brain regions of NMRs.

PPARs have distinct functions in the brain. PPARα controls the regulation of genes coding proteins that are involved in glutamate homeostasis and cholinergic/dopaminergic signaling.[49] In previous studies, PPARα was observed to be associated with calcium influx and the expression of several genes coding hippocampal proteins involved in the regulation of synaptic plasticity and involved in the expression of *N*-methyl-D-aspartate (NMDA) receptor subunit GRIN2A and GRIN2B and 2-amino-3(3-hydroxy-5-methyl-isoxasol-4-yl) propanoic acid (AMPA) receptor-associated subunit GRIA1.[50] Here, we observed a decrease of NMDA receptor subunits GRIN1 and GRIN2B in all brain regions (cerebellum, cortex, and hippocampus), whereas GRIN2A was increased in the cerebellum and decreased in the hippocampus (Figure S11). Moreover, we also measured numerous AMPA receptor subunits, where we observed a decrease of GRIA1 in the hippocampus, a decrease of GRIA3 in the cerebellum and hippocampus, and a decrease of GRIA4 in the cerebellum and hippocampus (Figure S12). Our results suggest that activation of PPARα may be enhanced in the cerebellum of NMRs compared to mice given the increased expression of FABP3. On the other hand, PPARβ has been observed to be directly involved in neuronal differentiation.[51] Our data indicate a decrease in its transcriptional activator FABP5 in all tissues in NMRs, suggesting that activation of this receptor may be repressed. This is an interesting observation and suggests that the rate of neuronal differentiation in NMRs may be decreased relative to mice. Additionally, PPARγ regulates the expression of genes coding enzymes engaged in amyloid precursor protein (APP) metabolism.[52] PPARγ is also thought to have tissue-specific effects; however, its activation is generally implicated in the regulation of cellular differentiation, lipid metabolism (including fatty acids), and glucose homeostasis.[53] Remarkably, PPARγ ligands are thought to attenuate degenerative processes in the brain and have been associated with the activation of anti-inflammatory mechanisms, oxidative stress, neurogenesis, and neuronal differentiation.[54,55] Taken together, we hypothesize that activation of PPARα and PPARγ are enhanced in NMR brains, representing different neuroprotective mechanisms, such as those needed under oxygen-deprived conditions. Considering that PPARα and PPARγ are known to regulate transcription of a vast array of genes, the predictive outcome of PPAR activation in the brain may encompass a very broad range of enhanced biological functions in NMRs compared to mice including calcium signaling,

https://doi.org/10.1021/acs.jproteome.1c00131
J. Proteome Res. XXXX, XXX, XXX−XXX

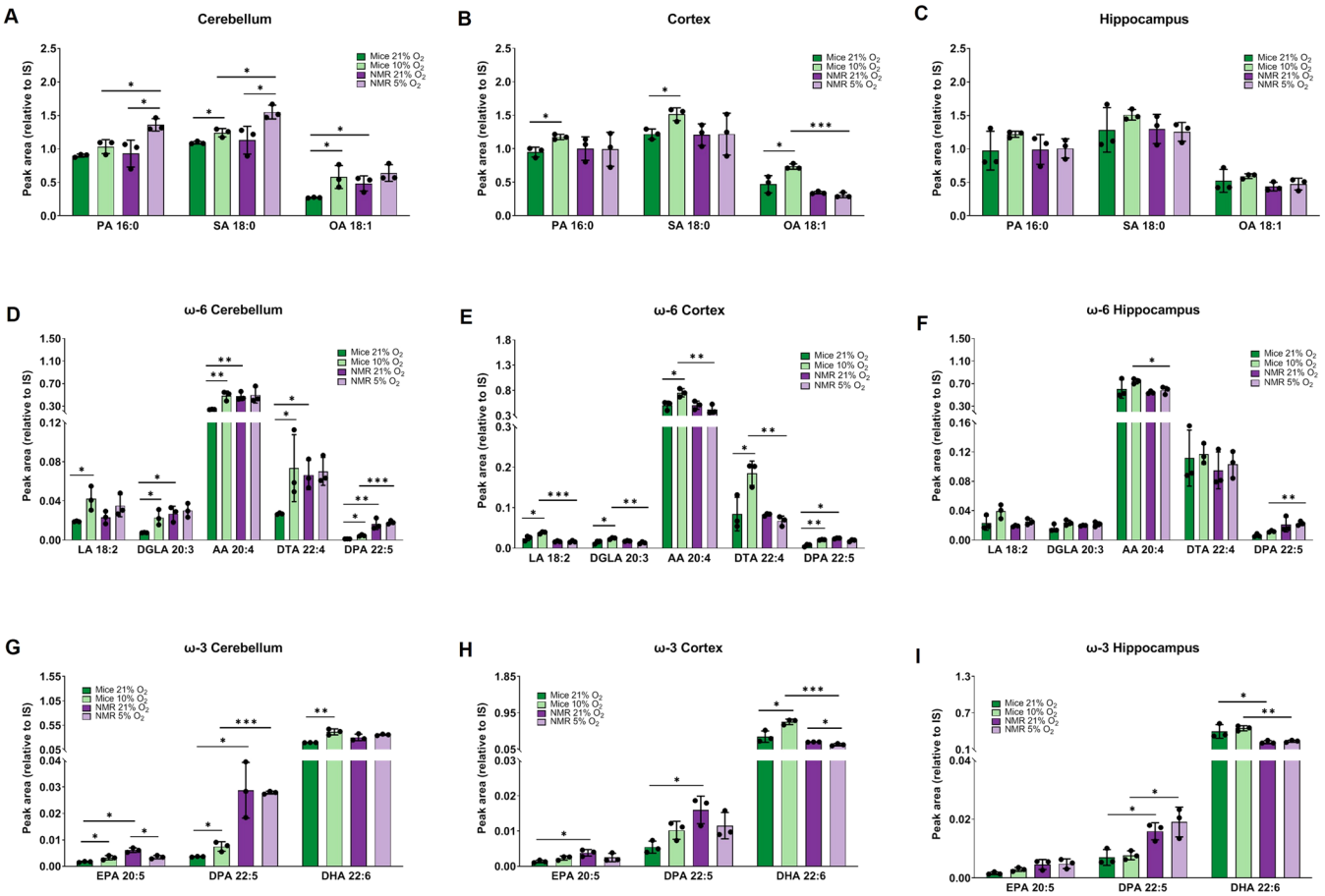

Figure 5. Fatty acids in the brain tissue of mice and naked mole-rats under normal and hypoxic conditions. Fatty acid levels were measured for animals held at normoxic (21% O_2) and hypoxic conditions for both mice (10% O_2) and naked mole-rats (NMR) (5% O_2) across different brain regions. Relative levels of PA, SA, and OA are shown in (A) cerebellum, (B) cortex, and (C) hippocampus tissues. Relative levels of LA, DGLA, AA, DTA, and ω-6 DPA were measured in the (D) cerebellum, (E) cortex, and (F) hippocampus tissues. Relative levels of EPA, DHA, ω-3 DPA were measured in the (G) cerebellum, (H) cortex, and (I) hippocampus tissues. Peak areas for all fatty acids were normalized to a PA-d_3 internal standard. Significance was determined via an unpaired *t*-test between all possible pairs of conditions in each (A)−(I) and noted as $p \leq 0.05$ (*), $p \leq 0.01$ (**), and $p \leq 0.001$ (***).

neuronal repair, and synaptic plasticity; however, further studies would be needed to explore these mechanisms in more detail. Additionally, we consider that activation of PPARβ may be repressed in NMRs, indicating that the rate of neuronal differentiation may be decreased in NRMs relative to mice.

Given the link between fatty acid-binding proteins and PPARs, we compared the relative levels of selected FABPs in NMRs and mice under normoxic and hypoxic conditions. Western blot analysis revealed a decrease in FABP5 across all brain regions (Figure S13, Figure 4A), although only statistically significant in the cortex. This data supports the notion that PPARβ activation is repressed by FABP5 in the brains of NMRs. On the other hand, we observed an increase in FABP3 in both the cerebellum and cortex (Figure S14, Figure 4B), although only significant in the cerebellum. Also, we observed a significant increase of FABP4 in both the cerebellum and cortex (Figure S15, Figure 4C). Under hypoxic conditions, we observed a larger increase in FABP3 in mice, whereas levels in NMR were more comparable to basal levels. Interestingly, the levels of FAPB4 did not increase with such a magnitude as FABP3 in mice under hypoxic conditions, suggesting that PPARα activation may be enhanced, much greater than PPARγ activation under oxygen-deprived conditions in mice. Interestingly, we do not observe a significant increase in FABP3 or FABP4 in NMRs, suggesting that they may have an innate activation of PPARα and PPARγ, even in control animals. Together, these data may represent one way by which NMRs have adapted to survive their oxygen-deprived burrows.

Fatty Acid Alterations Related to Oxygen Deprivation

In addition to their implication in the detoxification of ROS, fatty acids are also involved in maintaining other aspects of brain function, particularly neurotransmission. Interestingly, the anti-inflammatory and antioxidant properties of the PUFAs has been implicated in the preservation of neurological tissue during ischemic conditions.[56] Remarkably, Jiang and colleagues showed a reduction of stroke-induced neurological deficits with post-treatment of omega-3, where these PUFAs enhanced angiogenesis, oligodendrogenesis, neuron survival and white matter restoration.[57] Given that PUFAs are known to bind to PPAR nuclear receptors and are implicated in neuronal survival, we sought to evaluate the levels of selected fatty acids across different brain regions of NMRs and mice under normoxic and hypoxic conditions.

We measured fatty acid levels for animals held at normoxic and hypoxic conditions for both mice (10% O_2) and NMRs

https://doi.org/10.1021/acs.jproteome.1c00131
J. Proteome Res. XXXX, XXX, XXX−XXX

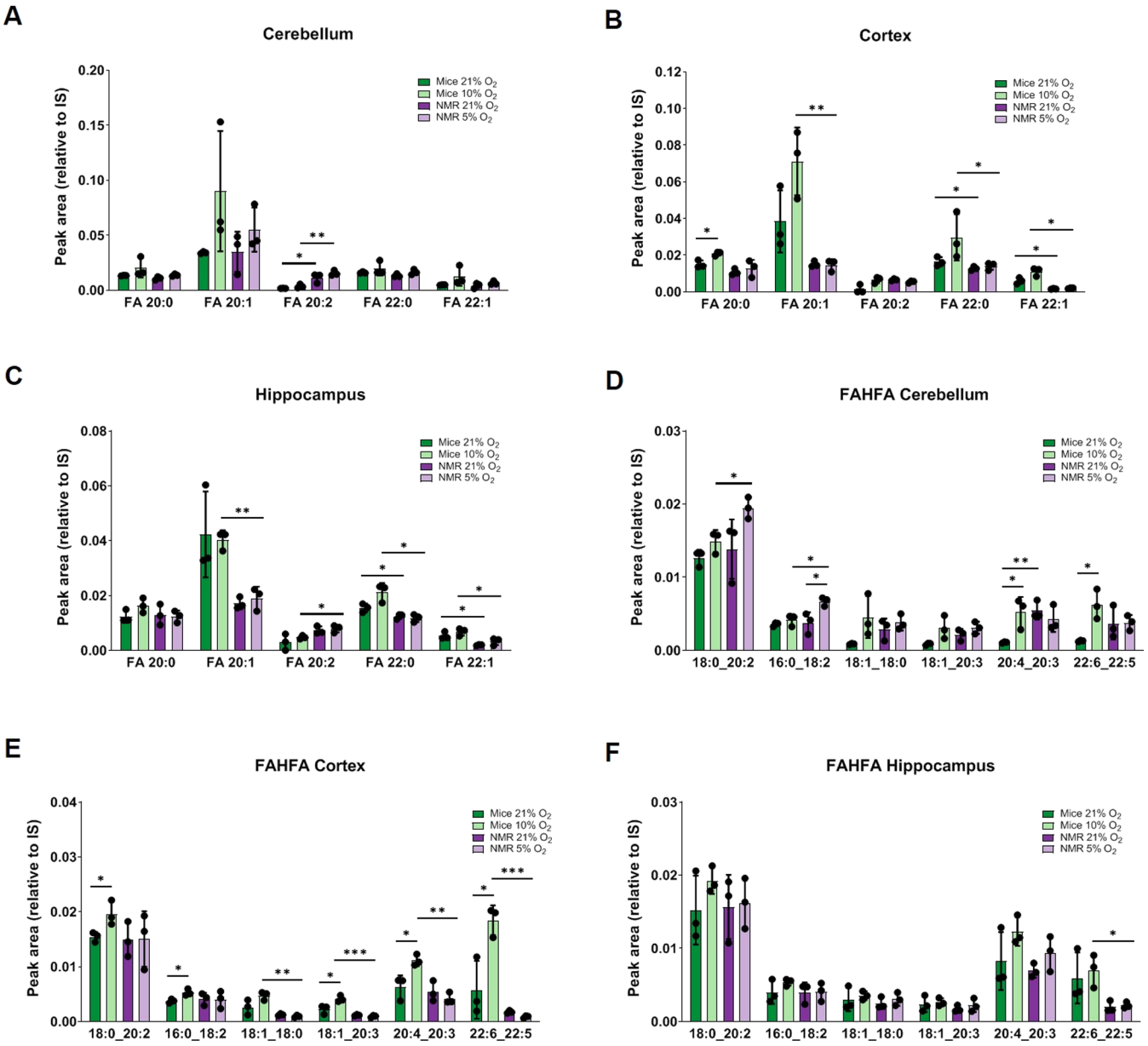

Figure 6. Untargeted analysis of fatty acid levels measured in the brain of mice and naked mole-rats under normoxic and hypoxic conditions. An untargeted liquid chromatography-mass spectrometry (LC-MS) analysis for fatty acid was carried out for animals held at normoxic (21% O_2) and hypoxic conditions for both mice (10% O_2) and naked mole-rats (NMR, 5% O_2) species. Relative levels of fatty acid species 20:0, 20:1, 20:2, 22:0, and 22:1 in the (A) cerebellum, (B) cortex, and (C) hippocampus are shown. Numerous fatty acid esters of hydroxyl fatty acids (FAHFA) were observed in the (D) cerebellum, (E) cortex, and (F) hippocampus. Peak areas for all fatty acids were normalized to a deuterated palmitic acid internal standard. Significance was determined via an unpaired t-test between all possible pairs of conditions in each (A)−(F) and noted as $p \leq 0.05$ (*), $p \leq 0.01$ (**), and $p \leq 0.001$ (***).

(5% O_2). First, relative levels of PA, SA, and OA acid were measured in the cerebellum, cortex, and hippocampus (Figure 5A−C). No alterations in PA, SA, or OA were observed in the hippocampus of either species under normoxic or hypoxic conditions. Under normoxic conditions, we observed an increase in OA in the cerebellum in NMRs. Under hypoxic conditions, mice show an increase in fatty acid levels in both the cerebellum and cortex, except PA which was not significant in the cerebellum. Under hypoxic conditions, NMRs also show an increase of PA and SA only in the cerebellum. Additionally, the levels of PA and SA were observed to be higher in NMRs relative to mice in the cerebellum under hypoxic conditions. Next, relative levels of omega (ω)-6 fatty acids LA, DGLA, AA, DTA, and ω-6 DPA were measured in cerebellum, cortex, and hippocampus (Figure 5D−F) tissues. Under normoxic conditions, an increase in DGLA, AA, DTA, and DPA was only observed in the cerebellum in NMRs compared to mice. Under hypoxic conditions, mice show an increase in ω-6 fatty acid levels in both the cerebellum and cortex, while the hippocampus shows no significant changes. Interestingly, no changes in ω-6 fatty acid levels were observed for NMRs under hypoxic conditions across any of the brain regions (Figure 5D−F). Additionally, under hypoxic conditions, more ω-6 DPA and less LA, DGLA, AA, and DTA were observed in the cortex for NMRs compared to mice. Less AA and more ω-6 DPA in the hippocampus were observed in NMRs under

https://doi.org/10.1021/acs.jproteome.1c00131
J. Proteome Res. XXXX, XXX, XXX−XXX

hypoxic conditions. Finally, relative levels of omega (ω)-3 fatty acids EPA, DHA, and ω-3 DPA were measured in the cerebellum, cortex, and hippocampus (Figure 5G−I) tissues. Under normoxic conditions, increased EPA in the cerebellum and cortex was observed and ω-3 DPA was increased in all tissue types for NMRs compared to mice. Under hypoxic conditions, mice display an increase in ω-3 fatty acid levels in the cerebellum and an increase in DHA in the cortex. Under hypoxic conditions, NMRs show a decrease of EPA in the cerebellum and DHA in the cortex, while no changes were observed in the hippocampus. Also, under hypoxic conditions, we observed that NMR tissues have higher ω-3 DPA in the cerebellum and hippocampus and lower DHA levels in the cortex and hippocampus compared to mice. With this, we conclude that NMRs have increased basal levels of EPA and ω-3 DPA compared to mice, where levels do not change under oxygen-deprived conditions.

Overall, we see an increase in multiple fatty acids levels in mice in both the cerebellum and cortex during periods of oxygen deprivation, observing a similar trend in the hippocampus although not significant. This observation may indicate that the hippocampal region requires a longer exposure to obtain the same significant difference, given that each tissue region is comprised of different cell types. Under hypoxic conditions, we only see a slight increase of PA and SA limited to the cerebellum. Interestingly, we did not observe an increase in the most common PUFAs, AA, or DHA. On the other hand, the cerebellum and cortex basal levels of EPA and ω-3 DPA were much higher in NMRs across brain regions, increasing under hypoxic conditions in mice and remaining unchanged in NMRs. The altered basal levels are consistent with previous observations in NMRs.[17] We posit that these omega-3 fatty acids may play an important role in maintaining neuronal integrity during periods of oxygen deprivation, a condition in which NRMs are known to tolerate. Given our pathway analysis of increased RXR signaling and alterations in FABPs and that FABPs have a broad specificity for long-chain fatty acids, we believe that FABP3 and FABP4 may be able to transport EPA and ω-3 DPA into the nucleus and selectively activate PPARα and PPARγ under conditions of oxygen deprivation, thereby activating neuronal protective mechanisms. Activation of PPARα and PPARγ could possibly explain, in part, why NMRs are able to maintain synaptic function and change their mitochondrial metabolism under hypoxic conditions[3] and why NMR brains are not observed to contain amyloid plaques.[24]

Commonly, the most abundant fatty acids chains are measured in biological systems. To identify and evaluate the relative abundance of less common fatty acids, an untargeted LC-MS analysis was carried out for NMRs and mice under both noroxic and hypoxic conditions. Here, relative intensities for fatty acid species 20:0, 20:1, 20:2, 22:0, and 22:1 were measured in the cerebellum, cortex, and hippocampus (Figure 6A−C) tissues. Under normoxic conditions, 20:2 was increased in the cerebellum and 22:0 increased in the cortex and hippocampus of NMR relative to mice. Under hypoxic conditions, only 20:0 was observed to increase in the cortex of the mice, while NMRs remained unchanged. Under hypoxic conditions, NMRs were observed to have more 20:2 in the cerebellum and hippocampus and less 20:1 and 22:0 in the cortex and hippocampus. In this study, numerous fatty acid esters of hydroxyl fatty acids (FAHFA) were also identified in the cerebellum, cortex, and hippocampus (Figure 6D−F) tissues. Under normoxic conditions, an increase in basal levels of 20:4_20:3 FAHFA was shown only in the cerebellum of NMRs, while all of the other FAHFAs showed no significant change. Under hypoxic conditions, mice show an increase in 20:4_20:3 in both the cerebellum and cortex. Additionally, 18:0_20:2, 16:0_18:2, 18:1_20:3, and 22:6_22:5 were also observed to be increased in the cortex of mice under hypoxic conditions. Under hypoxic conditions, NMRs only show an increase in 16:0_18:2 in the cerebellum. During hypoxia, NMRs show increased levels of 18:0_20:2 and 16:0_18:2 in the cerebellum while mice show increased levels of 18:0_18:0, 18:1_20:3, 20:4_20:3, and 20:6_20:5 in the cortex and 22:6_22:5 in both the cortex and hippocampus. To date, the biological function of these particular branched-chain fatty acids esters remains elusive; however, some studies have implicated them to have anti-inflammatory effects and regulators of metbolism,[58−60] perhaps also attributing to the NMR adaptive properties. Although the precise biological relevance of these changes is not currently transparent, the findings of our untargeted mass spectrometry analysis represent a unique subset of molecules that are altered in NMRs under normoxic and hypoxic conditions.

CONCLUSIONS

This study explores altered biomolecules in the brain of NMRs. Here, we describe our observations and highlight a potential mechanism by which neuronal integrity could possibly be maintained under limited oxygen conditions, such as those typically found in NMR burrows. Using mass spectrometry, we evaluated the altered proteome in NMRs relative to mice. Here, we observed numerous proteomic changes which suggest that the mitochondria of NMRs may have evolved to survive their environment. Additionally, our proteomic analysis suggests a decreased population of astrocytes across all regions of NMR brains. Building on our proteomic observations, we also explored DHA and AA peroxidation and found that NMRs do not undergo lipid peroxidation to the same extent as mice under oxygen-deprived conditions. Several lines of evidence also suggested that PPARα/γ-RXR signaling may be enhanced in NMRs. With this, we evaluated the levels of PUFAs and FABPs, which are known to enhance this signaling cascade. Here, we observed increased basal levels of EPA and ω-3 DPA in NMRs compared to mice, which did not change under oxygen-deprived conditions. Further mechanistic experiments are needed to explore the above speculated roles of EPA, ω-3 DPA, and the FAHFAs in NMRs and how they promote neuronal survival. Additionally, we observed an increase of known activators of PPARα and PPARγ (FABP3 and FABP4). Together these data suggest that PPAR signaling is enhanced in NMRs, possibly contributing to an intrinsic, neuronal protective mechanism.

ASSOCIATED CONTENT

Supporting Information

The Supporting Information is available free of charge at https://pubs.acs.org/doi/10.1021/acs.jproteome.1c00131.

Figure S1: Sample preparation and mass spectrometry analysis workflow; Figure S2: Summary of data analysis workflow; Table S1: Primary and secondary antibodies used for Western blot analysis; Figure S3: Standard curves for measuring lipid peroxidation products; Figure S4: Analysis of peroxidation products; Figure S5:

https://doi.org/10.1021/acs.jproteome.1c00131
J. Proteome Res. XXXX, XXX, XXX−XXX

Number of identified proteins in each species; Figure S6: Principle component analysis of altered proteins; Figure S7: Volcano plots; Figure S8: Ingenuity Pathway Analysis of the altered proteome observed between mice and naked mole-rats; Figure S9: Western blots for glial fibrillary acidic protein expression; Figure S10: The relative abundance of fatty acid-binding proteins measured by mass spectrometry; Figure S11: The relative abundance of NMDA receptor subunits measured by mass spectrometry; Figure S12: The relative abundance of AMPA/Glutamate receptor subunits measured by mass spectrometry; Figure S13: Western blots for fatty acid-binding protein 5; Figure S14: Western blots for fatty acid-binding protein 3; and Figure S15: Western blots for fatty acid-binding protein 4 (PDF)

Table S2: Mass spectrometry proteomic analysis (XLSX)

Table S3: Pathway analysis (XLS)

Table S4: Disease and biological function analysis (XLS)

AUTHOR INFORMATION

Corresponding Author

Stephanie M. Cologna − *Department of Chemistry, University of Illinois at Chicago, Chicago, Illinois 60607, United States; Laboratory for Integrative Neuroscience, University of Illinois at Chicago, Chicago, Illinois 60607, United States;* orcid.org/0000-0002-3541-3361; Phone: 312-413-2762; Email: cologna@uic.edu

Authors

Melissa R. Pergande − *Department of Chemistry, University of Illinois at Chicago, Chicago, Illinois 60607, United States*

Vince G. Amoroso − *Department of Biological Sciences, University of Illinois at Chicago, Chicago, Illinois 60607, United States*

Thu T. A. Nguyen − *Department of Chemistry, University of Illinois at Chicago, Chicago, Illinois 60607, United States*

Wenping Li − *Department of Chemistry, University of Illinois at Chicago, Chicago, Illinois 60607, United States*

Emily Vice − *Department of Biological Sciences, University of Illinois at Chicago, Chicago, Illinois 60607, United States*

Thomas J. Park − *Department of Biological Sciences and Laboratory for Integrative Neuroscience, University of Illinois at Chicago, Chicago, Illinois 60607, United States*

Complete contact information is available at: https://pubs.acs.org/10.1021/acs.jproteome.1c00131

Notes

The authors declare no competing financial interest.

ACKNOWLEDGMENTS

This work was supported by the Department of Chemistry, College of Liberal Arts and Sciences, University of Illinois at Chicago. Financial support from Diversifying Faculty in Illinois (to M.R.P.) is acknowledged. The authors acknowledge support from the National Science Foundation (1655494) (to S.M.C. and T.J.P.). The authors are also grateful for support from the Ara Parseghian Medical Research Fund University of Notre Dame, South Bend, Indiana.

REFERENCES

(1) Jarvis, J. U. Eusociality in a mammal: cooperative breeding in naked mole-rat colonies. *Science* **1981**, *212*, 571−3.

(2) Fang, X.; Seim, I.; Huang, Z.; Gerashchenko, M. V.; Xiong, Z.; Turanov, A. A.; Zhu, Y.; Lobanov, A. V.; Fan, D.; Yim, S. H.; Yao, X.; Ma, S.; Yang, L.; Lee, S. G.; Kim, E. B.; Bronson, R. T.; Šumbera, R.; Buffenstein, R.; Zhou, X.; Krogh, A.; Park, T. J.; Zhang, G.; Wang, J.; Gladyshev, V. N. Adaptations to a subterranean environment and longevity revealed by the analysis of mole rat genomes. *Cell Rep.* **2014**, *8*, 1354−64.

(3) Park, T. J.; Reznick, J.; Peterson, B. L.; Blass, G.; Omerbašić, D.; Bennett, N. C.; Kuich, P.; Zasada, C.; Browe, B. M.; Hamann, W.; Applegate, D. T.; Radke, M. H.; Kosten, T.; Lutermann, H.; Gavaghan, V.; Eigenbrod, O.; Bégay, V.; Amoroso, V. G.; Govind, V.; Minshall, R. D.; Smith, E. S. J.; Larson, J.; Gotthardt, M.; Kempa, S.; Lewin, G. R. Fructose-driven glycolysis supports anoxia resistance in the naked mole-rat. *Science* **2017**, *356*, 307−311.

(4) Larson, J.; Park, T. J. Extreme hypoxia tolerance of naked mole-rat brain. *NeuroReport* **2009**, *20*, 1634−7.

(5) Bennett, N.; Jarvis, J. U. M.; Davies, K. C. Daily and seasonal temperatures in the burrows of African rodent moles. *S. Afr. J. Zool.* **1988**, *23*, 189−195.

(6) Braude, S. African Mole-rats: Ecology and Eusociality. *Ethology* **2000**, *106*, 1046−1048.

(7) Ruby, J. G.; Smith, M.; Buffenstein, R. Naked Mole-Rat mortality rates defy gompertzian laws by not increasing with age. *eLife* **2018**, No. e31157.

(8) Jiang, J. J.; Kong, Q. P. Comparative analysis of long noncoding RNAs in long-lived mammals provides insights into natural cancer-resistance. *RNA Biol.* **2020**, *17*, 1657−1665.

(9) Kim, E. B.; Fang, X.; Fushan, A. A.; Huang, Z.; Lobanov, A. V.; Han, L.; Marino, S. M.; Sun, X.; Turanov, A. A.; Yang, P.; Yim, S. H.; Zhao, X.; Kasaikina, M. V.; Stoletzki, N.; Peng, C.; Polak, P.; Xiong, Z.; Kiezun, A.; Zhu, Y.; Chen, Y.; Kryukov, G. V.; Zhang, Q.; Peshkin, L.; Yang, L.; Bronson, R. T.; Buffenstein, R.; Wang, B.; Han, C.; Li, Q.; Chen, L.; Zhao, W.; Sunyaev, S. R.; Park, T. J.; Zhang, G.; Wang, J.; Gladyshev, V. N. Genome sequencing reveals insights into physiology and longevity of the naked mole rat. *Nature* **2011**, *479*, 223−7.

(10) Zhou, X.; Dou, Q.; Fan, G.; Zhang, Q.; Sanderford, M.; Kaya, A.; Johnson, J.; Karlsson, E. K.; Tian, X.; Mikhalchenko, A.; Kumar, S.; Seluanov, A.; Zhang, Z. D.; Gorbunova, V.; Liu, X.; Gladyshev, V. N. Beaver and Naked Mole Rat Genomes Reveal Common Paths to Longevity. *Cell Rep.* **2020**, *32*, No. 107949.

(11) Lewis, K. N.; Andziak, B.; Yang, T.; Buffenstein, R. The naked mole-rat response to oxidative stress: just deal with it. *Antioxid. Redox Signaling* **2013**, *19*, 1388−99.

(12) Munro, D.; Baldy, C.; Pamenter, M. E.; Treberg, J. R. The exceptional longevity of the naked mole-rat may be explained by mitochondrial antioxidant defenses. *Aging Cell* **2019**, *18*, No. e12916.

(13) Saldmann, F.; Viltard, M.; Leroy, C.; Friedlander, G. The Naked Mole Rat: A Unique Example of Positive Oxidative Stress. *Oxid. Med. Cell. Longevity* **2019**, *2019*, 1−7.

(14) Triplett, J. C.; Tramutola, A.; Swomley, A.; Kirk, J.; Grimes, K.; Lewis, K.; Orr, M.; Rodriguez, K.; Cai, J.; Klein, J. B.; Perluigi, M.; Buffenstein, R.; Butterfield, D. A. Age-related changes in the proteostasis network in the brain of the naked mole-rat: Implications promoting healthy longevity. *Biochim. Biophys. Acta, Mol. Basis Dis.* **2015**, *1852*, 2213−24.

(15) Triplett, J. C.; Swomley, A. M.; Kirk, J.; Grimes, K. M.; Lewis, K. N.; Orr, M. E.; Rodriguez, K. A.; Cai, J.; Klein, J. B.; Buffenstein, R.; Butterfield, D. A. Reaching Out to Send a Message: Proteins Associated with Neurite Outgrowth and Neurotransmission are Altered with Age in the Long-Lived Naked Mole-Rat. *Neurochem. Res.* **2016**, *41*, 1625−34.

(16) Heinze, I.; Bens, M.; Calzia, E.; Holtze, S.; Dakhovnik, O.; Sahm, A.; Kirkpatrick, J. M.; Szafranski, K.; Romanov, N.; Sama, S. N.; Holzer, K.; Singer, S.; Ermolaeva, M.; Platzer, M.; Hildebrandt, T.;

Ori, A. Species comparison of liver proteomes reveals links to naked mole-rat longevity and human aging. *BMC Biol.* **2018**, *16*, No. 82.
(17) Frankel, D.; Davies, M.; Bhushan, B.; Kulaberoglu, Y.; Urriola-Munoz, P.; Bertrand-Michel, J.; Pergande, M. R.; Smith, A. A.; Preet, S.; Park, T. J.; Vendruscolo, M.; Rankin, K. S.; Cologna, S. M.; Kumita, J. R.; Cenac, N.; St John Smith, E. Cholesterol-rich naked mole-rat brain lipid membranes are susceptible to amyloid beta-induced damage in vitro. *Aging* **2020**, *12*, 22266−22290.
(18) Gaun, A.; Lewis Hardell, K. N.; Olsson, N.; O'Brien, J. J.; Gollapudi, S.; Smith, M.; McAlister, G.; Huguet, R.; Keyser, R.; Buffenstein, R.; McAllister, F. E. Automated 16-Plex Plasma Proteomics with Real-Time Search and Ion Mobility Mass Spectrometry Enables Large-Scale Profiling in Naked Mole-Rats and Mice. *J. Proteome Res.* **2021**, *20*, 1280−1295.
(19) Pergande, M. R.; Nguyen, T. T. A.; Haney-Ball, C.; Davidson, C. D.; Cologna, S. M. Quantitative, Label-Free Proteomics in the Symptomatic Niemann-Pick, Type C1 Mouse Model Using Standard Flow Liquid Chromatography and Thermal Focusing Electrospray Ionization. *Proteomics* **2019**, *19*, No. 1800432.
(20) Pergande, M. R.; Zarate, E.; Haney-Ball, C.; Davidson, C. D.; Scesa, G.; Givogri, M. I.; Bongarzone, E. R.; Cologna, S. M. Standard-flow LC and thermal focusing ESI elucidates altered liver proteins in late stage Niemann-Pick, type C1 disease. *Bioanalysis* **2019**, *11*, 1067−1083.
(21) St John Smith, E.; Park, T. J. Neurobiology: Crowdsourcing CO(2) to Conserve Brain Energy. *Curr. Biol.* **2020**, *30*, R649−r651.
(22) Lewis, K. N.; Soifer, I.; Melamud, E.; Roy, M.; McIsaac, R. S.; Hibbs, M.; Buffenstein, R. Unraveling the message: insights into comparative genomics of the naked mole-rat. *Mamm. Genome* **2016**, *27*, 259−278.
(23) Yang, B.; Li, R.; Michael Greenlief, C.; Fritsche, K. L.; Gu, Z.; Cui, J.; Lee, J. C.; Beversdorf, D. Q.; Sun, G. Y. Unveiling anti-oxidative and anti-inflammatory effects of docosahexaenoic acid and its lipid peroxidation product on lipopolysaccharide-stimulated BV-2 microglial cells. *J. Neuroinflammation* **2018**, *15*, No. 202.
(24) Edrey, Y. H.; Medina, D. X.; Gaczynska, M.; Osmulski, P. A.; Oddo, S.; Caccamo, A.; Buffenstein, R. Amyloid beta and the longest-lived rodent: the naked mole-rat as a model for natural protection from Alzheimer's disease. *Neurobiol. Aging* **2013**, *34*, 2352−60.
(25) Pamenter, M. E.; Lau, G. Y.; Richards, J. G.; Milsom, W. K. Naked mole rat brain mitochondria electron transport system flux and H+ leak are reduced during acute hypoxia. *J. Exp. Biol.* **2018**, *221*, No. jeb171397.
(26) Yang, Q.; Zhou, Y.; Sun, Y.; Luo, Y.; Shen, Y.; Shao, A. Will Sirtuins Be Promising Therapeutic Targets for TBI and Associated Neurodegenerative Diseases? *Front. Neurosci.* **2020**, *14*, No. 791.
(27) Wang, Y.; Yang, J.; Hong, T.; Chen, X.; Cui, L. SIRT2: Controversy and multiple roles in disease and physiology. *Ageing Res. Rev.* **2019**, *55*, No. 100961.
(28) Mu, N.; Lei, Y.; Wang, Y.; Wang, Y.; Duan, Q.; Ma, G.; Liu, X.; Su, L. Inhibition of SIRT1/2 upregulates HSPA5 acetylation and induces pro-survival autophagy via ATF4-DDIT4-mTORC1 axis in human lung cancer cells. *Apoptosis* **2019**, *24*, 798−811.
(29) Xu, D.; Jiang, X.; He, H.; Liu, D.; Yang, L.; Chen, H.; Wu, L.; Geng, G.; Li, Q. SIRT2 functions in aging, autophagy, and apoptosis in post-maturation bovine oocytes. *Life Sci.* **2019**, *232*, No. 116639.
(30) Hawkins, L. J.; Hadj-Moussa, H.; Nguyen, V. C.; Pamenter, M. E.; Storey, K. B. Naked mole rats activate neuroprotective proteins during hypoxia. *J. Exp. Zool., Part A* **2019**, *331*, 571−576.
(31) Andziak, B.; O'Connor, T. P.; Qi, W.; DeWaal, E. M.; Pierce, A.; Chaudhuri, A. R.; Van Remmen, H.; Buffenstein, R. High oxidative damage levels in the longest-living rodent, the naked mole-rat. *Aging Cell* **2006**, *5*, 463−71.
(32) Liguori, I.; Russo, G.; Curcio, F.; Bulli, G.; Aran, L.; Della-Morte, D.; Gargiulo, G.; Testa, G.; Cacciatore, F.; Bonaduce, D.; Abete, P. Oxidative stress, aging, and diseases. *Clin. Interventions Aging* **2018**, *13*, 757−772.
(33) Penz, O. K.; Fuzik, J.; Kurek, A. B.; Romanov, R.; Larson, J.; Park, T. J.; Harkany, T.; Keimpema, E. Protracted brain development in a rodent model of extreme longevity. *Sci. Rep.* **2015**, *5*, No. 11592.
(34) Pérez, V. I.; Buffenstein, R.; Masamsetti, V.; Leonard, S.; Salmon, A. B.; Mele, J.; Andziak, B.; Yang, T.; Edrey, Y.; Friguet, B.; Ward, W.; Richardson, A.; Chaudhuri, A. Protein stability and resistance to oxidative stress are determinants of longevity in the longest-living rodent, the naked mole-rat. *Proc. Natl. Acad. Sci. USA* **2009**, *106*, 3059−64.
(35) Ioannou, M. S.; Jackson, J.; Sheu, S. H.; Chang, C. L.; Weigel, A. V.; Liu, H.; Pasolli, H. A.; Xu, C. S.; Pang, S.; Matthies, D.; Hess, H. F.; Lippincott-Schwartz, J.; Liu, Z. Neuron-Astrocyte Metabolic Coupling Protects against Activity-Induced Fatty Acid Toxicity. *Cell* **2019**, *177*, 1522−1535.e14.
(36) Behn, C.; Araneda, O.; Llanos, A.; Celedón, G.; Gonzalez, G. Hypoxia-related lipid peroxidation: Evidences, implications and approaches. *Respir. Physiol. Neurobiol.* **2007**, *158*, 143−50.
(37) Pham-Huy, L. A.; He, H.; Pham-Huy, C. Free radicals, antioxidants in disease and health. *Int. J. Biomed. Sci.* **2008**, *4*, 89−96.
(38) Sack, M. N. Mitochondrial depolarization and the role of uncoupling proteins in ischemia tolerance. *Cardiovasc. Res.* **2006**, *72*, 210−9.
(39) Mangelsdorf, D. J.; Evans, R. M. The RXR heterodimers and orphan receptors. *Cell* **1995**, *83*, 841−50.
(40) Clemens, V.; Regen, F.; Le Bret, N.; Heuser, I.; Hellmann-Regen, J. Anti-inflammatory effects of minocycline are mediated by retinoid signaling. *BMC Neurosci.* **2018**, *19*, 58.
(41) Klaassen, C. D.; Aleksunes, L. M. Xenobiotic, bile acid, and cholesterol transporters: function and regulation. *Pharmacol. Rev.* **2010**, *62*, 1−96.
(42) Ponsuksili, S.; Murani, E.; Brand, B.; Schwerin, M.; Wimmers, K. Integrating expression profiling and whole-genome association for dissection of fat traits in a porcine model. *J. Lipid Res.* **2011**, *52*, 668−78.
(43) Saijo, K.; Crotti, A.; Glass, C. K. Nuclear receptors, inflammation, and neurodegenerative diseases. *Adv. Immunol.* **2010**, *106*, 21−59.
(44) Skerrett, R.; Malm, T.; Landreth, G. Nuclear receptors in neurodegenerative diseases. *Neurobiol. Dis.* **2014**, *72 Pt A*, 104−16.
(45) Kliewer, S. A.; Sundseth, S. S.; Jones, S. A.; Brown, P. J.; Wisely, G. B.; Koble, C. S.; Devchand, P.; Wahli, W.; Willson, T. M.; Lenhard, J. M.; Lehmann, J. M. Fatty acids and eicosanoids regulate gene expression through direct interactions with peroxisome proliferator-activated receptors alpha and gamma. *Proc. Natl. Acad. Sci. USA* **1997**, *94*, 4318−23.
(46) Krey, G.; Braissant, O.; L'Horset, F.; Kalkhoven, E.; Perroud, M.; Parker, M. G.; Wahli, W. Fatty acids, eicosanoids, and hypolipidemic agents identified as ligands of peroxisome proliferator-activated receptors by coactivator-dependent receptor ligand assay. *Mol. Endocrinol.* **1997**, *11*, 779−91.
(47) Hsu, K. T.; Storch, J. Fatty acid transfer from liver and intestinal fatty acid-binding proteins to membranes occurs by different mechanisms. *J. Biol. Chem.* **1996**, *271*, 13317−23.
(48) Tan, N. S.; Shaw, N. S.; Vinckenbosch, N.; Liu, P.; Yasmin, R.; Desvergne, B.; Wahli, W.; Noy, N. Selective cooperation between fatty acid binding proteins and peroxisome proliferator-activated receptors in regulating transcription. *Mol. Cell. Biol.* **2002**, *22*, 5114−27.
(49) Wójtowicz, S.; Strosznajder, A. K.; Jeżyna, M.; Strosznajder, J. B. The Novel Role of PPAR Alpha in the Brain: Promising Target in Therapy of Alzheimer's Disease and Other Neurodegenerative Disorders. *Neurochem. Res.* **2020**, *45*, 972−988.
(50) Roy, A.; Jana, M.; Corbett, G. T.; Ramaswamy, S.; Kordower, J. H.; Gonzalez, F. J.; Pahan, K. Regulation of cyclic AMP response element binding and hippocampal plasticity-related genes by peroxisome proliferator-activated receptor α. *Cell Rep.* **2013**, *4*, 724−37.
(51) Di Loreto, S.; D'Angelo, B.; D'Amico, M. A.; Benedetti, E.; Cristiano, L.; Cinque, B.; Cifone, M. G.; Cerù, M. P.; Festuccia, C.;

https://doi.org/10.1021/acs.jproteome.1c00131
J. Proteome Res. XXXX, XXX, XXX−XXX

Cimini, A. PPARbeta agonists trigger neuronal differentiation in the human neuroblastoma cell line SH-SY5Y. *J. Cell. Physiol.* **2007**, *211*, 837−47.
(52) Govindarajulu, M.; Pinky, P. D.; Bloemer, J.; Ghanei, N.; Suppiramaniam, V.; Amin, R. Signaling Mechanisms of Selective PPARγ Modulators in Alzheimer's Disease. *PPAR Res.* **2018**, *2018*, No. 2010675.
(53) Ahmadian, M.; Suh, J. M.; Hah, N.; Liddle, C.; Atkins, A. R.; Downes, M.; Evans, R. M. PPARγ signaling and metabolism: the good, the bad and the future. *Nat. Med.* **2013**, *19*, 557−66.
(54) Villapol, S. Roles of Peroxisome Proliferator-Activated Receptor Gamma on Brain and Peripheral Inflammation. *Cell. Mol. Neurobiol.* **2018**, *38*, 121−132.
(55) Kersten, S.; Desvergne, B.; Wahli, W. Roles of PPARs in health and disease. *Nature* **2000**, *405*, 421−4.
(56) Zirpoli, H.; Chang, C. L.; Carpentier, Y. A.; Michael-Titus, A. T.; Ten, V. S.; Deckelbaum, R. J. Novel Approaches for Omega-3 Fatty Acid Therapeutics: Chronic Versus Acute Administration to Protect Heart, Brain, and Spinal Cord. *Annu. Rev. Nutr.* **2020**, *40*, 161−187.
(57) Jiang, X.; Suenaga, J.; Pu, H.; Wei, Z.; Smith, A. D.; Hu, X.; Shi, Y.; Chen, J. Post-stroke administration of omega-3 polyunsaturated fatty acids promotes neurovascular restoration after ischemic stroke in mice: Efficacy declines with aging. *Neurobiol. Dis.* **2019**, *126*, 62−75.
(58) Brejchova, K.; Balas, L.; Paluchova, V.; Brezinova, M.; Durand, T.; Kuda, O. Understanding FAHFAs: From structure to metabolic regulation. *Prog. Lipid Res.* **2020**, *79*, No. 101053.
(59) Kuda, O.; Brezinova, M.; Rombaldova, M.; Slavikova, B.; Posta, M.; Beier, P.; Janovska, P.; Veleba, J.; Kopecky, J., Jr.; Kudova, E.; Pelikanova, T.; Kopecky, J. Docosahexaenoic Acid-Derived Fatty Acid Esters of Hydroxy Fatty Acids (FAHFAs) With Anti-inflammatory Properties. *Diabetes* **2016**, *65*, 2580−90.
(60) Hernández-Saavedra, D.; Stanford, K. I. The Regulation of Lipokines by Environmental Factors. *Nutrients* **2019**, *11*, No. 2422.

https://doi.org/10.1021/acs.jproteome.1c00131
J. Proteome Res. XXXX, XXX, XXX−XXX